

Adaptive Nonlinear MPC for Trajectory Tracking of An Overactuated Tiltrotor Hexacopter

Yueqian Liu¹, Fengyu Quan² and Haoyao Chen²

Abstract—Omnidirectional micro aerial vehicles (OMAVs) are more capable of doing environmentally interactive tasks due to their ability to exert full wrenches while maintaining stable poses. However, OMAVs often incorporate additional actuators and complex mechanical structures to achieve omnidirectionality. Obtaining precise mathematical models is difficult, and the mismatch between the model and the real physical system is not trivial. The large model-plant mismatch significantly degrades overall system performance if a non-adaptive model predictive controller (MPC) is used. This work presents the \mathcal{L}_1 -MPC, an adaptive nonlinear model predictive controller for accurate 6-DOF trajectory tracking of an overactuated tiltrotor hexacopter in the presence of model uncertainties and external disturbances. The \mathcal{L}_1 -MPC adopts a cascaded system architecture in which a nominal MPC is followed and augmented by an \mathcal{L}_1 adaptive controller. The proposed method is evaluated against the non-adaptive MPC, the EKF-MPC, and the PID method in both numerical and PX4 software-in-the-loop simulation with Gazebo. The \mathcal{L}_1 -MPC reduces the tracking error by around 90% when compared to a non-adaptive MPC, and the \mathcal{L}_1 -MPC has lower tracking errors, higher uncertainty estimation rates, and less tuning requirements over the EKF-MPC. We will make the implementations, including the hardware-verified PX4 firmware and Gazebo plugins, open-source at <https://github.com/HITSZ-NRSL/omniHex>.

I. INTRODUCTION

A. Background

The past few years have seen much research and development around micro aerial vehicles (MAVs). MAVs are widely used in passive tasks, including aerial filming, rescuing, and terrain mapping. In these tasks, no physical interaction with the environment is required. For interactive tasks such as structure and material inspection, aerial manipulation, and wall painting, omnidirectional MAVs have been developed as they can generate full wrenches on their end effectors.

Different approaches for achieving omnidirectionality have been presented [1]. One approach stands out because of its optimized efficiency, where rotor tilting mechanisms are added to a regular fixed rotor hexacopter. The tilting mechanisms bring over-actuation and omnidirectionality to the system. So, we refer to an OMAV designed in such an approach as an overactuated tiltrotor hexacopter, and we name our OMAV model Omnihex.

This work was supported in part by the National Natural Science Foundation of China under Grant U1713206 and 61673131. The corresponding author is Haoyao Chen.

¹Yueqian Liu was with nROS-Lab. He is now with the Faculty of Aerospace Engineering, Delft University of Technology, Delft, 2629 HS, the Netherlands. Y.Liu-133@student.tudelft.nl

²Fengyu Quan and Haoyao Chen are with nROS-Lab, the School of Mechanical Engineering and Automation, Harbin Institute of Technology, Shenzhen, 518055, People's Republic of China. {18b353011@stu, hychen5@}.hit.edu.cn



Fig. 1. The Omnihex tracking a 6-DOF trajectory using our customized PX4 firmware.

The Omnihex can efficiently generate a desirable wrench envelope. However, the system is difficult to model since complicated dynamics may arise from tilting rotors, airflow turbulence, and other moving mechanical parts. Accurate trajectory tracking ability is fundamental for completing environmentally interactive and non-interactive tasks. Model predictive control proves an effective method for trajectory tracking tasks. However, the performance of MPC degrades when significant model mismatches exist. To compensate for the model mismatch and external disturbances that may act on the system during tasks requiring physical interaction with the environment, we augment the nominal MPC with the \mathcal{L}_1 adaptive control method to achieve accurate trajectory tracking.

B. Related Works

The overactuated tiltrotor hexacopter with six independent arm tilting mechanisms is first developed in [2]. The actuator effectiveness model, a least-energy control allocation method, and a basic control design for their OMAV, Voliro, have been presented. Voliro has been studied more extensively regarding hardware design, system modeling, PID control, and control allocation in [3]. In [4], additional propellers have been introduced to reduce the gyroscopic effect, and rotor tilting mechanisms have been reworked to reduce system inertia on their new VoliroX. Also, singularities of control allocation have been studied, and corresponding handling methods have been developed.

Many approaches have been presented to improve the control performance of VoliroX. In [5], jerk-level LQRI has

been derived alongside a new control allocation algorithm called differential allocation that can exploit the actuation null space. Learning the plant-model mismatch offline using a Gaussian process regressor also boosts controller performance [6]. However, the learned model should be updated whenever the system parameters change due to extra payloads, changes in battery specifications, or even repairs after damage. Furthermore, another limitation is that it cannot adapt to external disturbances during flights.

Trajectory tracking EKF-MPC has been derived for VoliroX in [7]. EKF-MPC uses an extended Kalman filter to estimate wrench errors that appear due to model mismatch and external disturbances. Then the estimated wrench is fused into the MPC formulation to achieve adaptivity. For tracking a hybrid force and pose trajectory at the end effector in an aerial manipulation task, a hybrid NMPC has been proposed in [8]. The hybrid NMPC is built upon the EKF-MPC in previous work. End effector force and pose tracking is beyond the scope of discussion of this work, and we focus on accurate trajectory tracking of the platform itself during free flight.

Another approach to adaptivity is to add an adaptive control layer between the MPC and the plant. We design the layer according to the \mathcal{L}_1 adaptive control theory. The \mathcal{L}_1 adaptive control theory provides fast adaptation while the adaptation rate is decoupled from robustness [9]–[12]. A linear model MPC cascaded by a linear model \mathcal{L}_1 adaptive controller for quadrotor trajectory tracking has been presented in [13]. Because linear models have been used, controller performance is expected to degrade when the quadrotor is doing highly aggressive maneuvers. The \mathcal{L}_1 adaptive control theory has again been applied to a quadrotor by cascading a model predictive path integral (MPPI) controller with an \mathcal{L}_1 adaptive controller in [14]. Although in [14], the advantage of augmenting a predictive controller with an \mathcal{L}_1 adaptive layer is demonstrated, the computational overhead of the MPPI controller is often too heavy for onboard computers. With a focus on the agile and highly aggressive flight of quadrotors, work [15] presents \mathcal{L}_1 -NMPC, in which nonlinear models have been used for both controllers. Experiments in [15] show that tracking errors are reduced by a significant amount under large unknown disturbances and without any parameter tuning, even when quadrotors are flying highly agile racing trajectories. Notable works have been done on quadrotors, but to the best of our knowledge, \mathcal{L}_1 -MPC has not been derived for Omnihex yet.

C. Contribution

We present the \mathcal{L}_1 -MPC for accurate trajectory tracking of an overactuated tiltrotor hexacopter. The controller has the following favorable features:

- It adapts to changes in model parameters (vehicle mass, inertia, center of mass, and propeller coefficients) and time-variant external disturbances.
- Minimal computational overhead is introduced and the time required for solving an optimal control problem is reduced.

- Compared to a non-adaptive MPC with nominal model dynamics and parameters, it lowers tracking error by around 90%.

In addition, we will release an open-source simulation scheme and the verified PX4 firmware. These practical implementations can be used for verifying other novel algorithms and general Omnihex future developments, such as autonomous navigation in cluttered environments and cooperating with a robotic arm.

II. SYSTEM MODELING

A. Platform Overview

The Omnihex is a hexacopter with its arms tilted by six Dynamixel servos. The servos are placed in the center base. Unlike the VoliroX, which has two counter-rotating rotors per arm, the gyroscopic effect may be more evident on the Omnihex. Nevertheless, the gyroscopic effect is neglected in the nominal model since we use an adaptive design.

Coordinate systems are illustrated in fig. 2. We attach an FRD-XYZ body frame to the geometric center of the Omnihex. For the world frame, the NED-XYZ frame is used. The shown coordinate systems match the ones defined in the PX4 software.

B. Notations

Left subscripts denote coordinate frames: W for the world frame and B for the body frame. Right subscripts are abbreviations of value properties. Attitude quaternions are written as $\mathbf{q} = [w, x, y, z]^T$, where the scalar w is followed by the vector part $[x, y, z]$. The coordinate transformation of a vector in the body frame ${}_B\mathbf{v}$ to the world frame is given in (1) that uses the quaternion product \otimes :

$${}_W\mathbf{v} = \mathbf{q} \otimes {}_B\mathbf{v} \otimes \mathbf{q}^{-1} = \text{rotate}({}_B\mathbf{v}, \mathbf{q}) \quad (1)$$

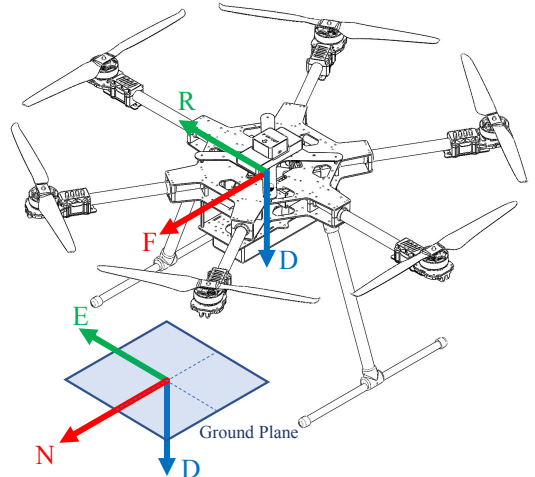


Fig. 2. Illustration of the Omnihex and frames.

C. Rigid Body Dynamics

We ignore the complex dynamics that result from moving parts and airflow interference, and we model the OmniHex as a rigid body. Rigid body dynamics consist of equations of kinematics, as well as equations for dynamics that are described using the Newton-Euler equation.

The equations for kinematics are based on the definition of velocity and the mapping from body angular velocity to quaternion rate [16]. As illustrated in fig. 3 and expressed by (2), the total wrench, ${}_B\mathbf{f}_{com}$ and ${}_B\boldsymbol{\tau}_{com}$, that acts on the center of gravity is used for bridging the Newton-Euler equation and the total wrench produced by actuators, ${}_B\mathbf{f}_a$ and ${}_B\boldsymbol{\tau}_a$.

$$\begin{bmatrix} m \cdot {}_W\dot{\mathbf{v}} \\ \mathbf{J} \cdot {}_B\dot{\boldsymbol{\omega}} + {}_B\boldsymbol{\omega} \times (\mathbf{J} \cdot {}_B\boldsymbol{\omega}) \end{bmatrix} = \begin{bmatrix} m\mathbf{g} + \text{rotate}({}_B\mathbf{f}_a, \mathbf{q}) \\ {}_B\boldsymbol{\tau}_a - {}_B\mathbf{d}_{com} \times {}_B\mathbf{f}_a \end{bmatrix} \quad (2)$$

Therefore, the complete rigid body dynamics equation is written as:

$$\begin{bmatrix} \dot{\mathbf{p}} \\ \dot{\mathbf{q}} \\ {}_W\dot{\mathbf{v}} \\ {}_B\dot{\boldsymbol{\omega}} \end{bmatrix} = \begin{bmatrix} {}_W\mathbf{v} \\ \frac{1}{2}\mathbf{q} \otimes \begin{bmatrix} 0 \\ {}_B\boldsymbol{\omega} \end{bmatrix} \\ \mathbf{g} + \frac{1}{m}\text{rotate}({}_B\mathbf{f}_a, \mathbf{q}) \\ \mathbf{J}^{-1}({}_B\boldsymbol{\tau}_a - {}_B\mathbf{d}_{com} \times {}_B\mathbf{f}_a - {}_B\boldsymbol{\omega} \times (\mathbf{J} \cdot {}_B\boldsymbol{\omega})) \end{bmatrix} \quad (3)$$

where m is the mass and \mathbf{J} is the inertia, ${}_W\mathbf{v}$ is the vehicle linear velocity and ${}_W\dot{\mathbf{v}}$ is the linear acceleration, \mathbf{g} is the gravitational acceleration, ${}_B\boldsymbol{\omega}$ is the body angular velocity and ${}_B\dot{\boldsymbol{\omega}}$ is the angular acceleration, ${}_B\mathbf{d}_{com}$ is the center of mass position relative to the body frame.

D. Actuator Effectiveness

Rotor spinning directions and the positive angle direction is shown in fig. 4. Rotor spinning directions are configured in such a way as to match the PX4 convention. The positive angle direction for each arm is determined by the other fingers of one's right hand, with the thumb pointing outwards from the center. The exact configuration has been used in [2], [3].

We assume that the forces and torques produced by tilting rotating propellers, including the gyroscopic effect, can be compensated by adaptive measures. Also, we assume that the

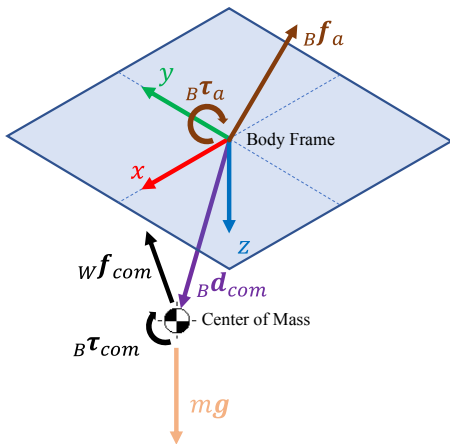


Fig. 3. Wrench analysis of the rigid body.

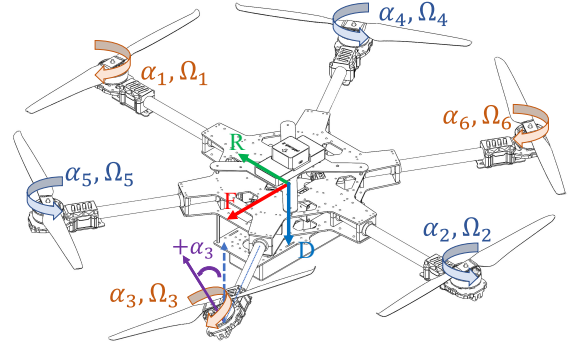


Fig. 4. Propeller spinning directions and positive tilting angle configuration.

servo can change the tilt angle arbitrarily fast. While ignoring the tilt dynamics, constraints on wrench changing rates are incorporated in the MPC design. With such assumptions, each propeller produces forces and torques proportional to the square of the rotor angular velocity. The force f_i and torque τ_i generated by rotor number i are:

$$f_i = \mu \Omega_i^2, \quad \tau_i = k \Omega_i^2 \quad (4)$$

where μ and k are coefficients that characterize the performance of a propeller and Ω_i is the angular velocity. The actuator effectiveness model is described by:

$$\begin{bmatrix} {}_B\mathbf{f}_{com} \\ {}_B\boldsymbol{\tau}_{com} \end{bmatrix} = \mathbf{M}[\Omega_1^2, \Omega_2^2, \Omega_3^2, \Omega_4^2, \Omega_5^2, \Omega_6^2]^\top \quad (5)$$

where matrix \mathbf{M} is a nonlinear function of μ , k , and six tilt angles $\alpha_1, \dots, \alpha_6$. \mathbf{M} is also referred to as the allocation matrix in [2] and [3], where its expression is presented in detail.

III. CONTROL DESIGN

A. \mathcal{L}_1 -MPC

The \mathcal{L}_1 adaptive control method is a kind of model reference adaptive control (MRAC) that features decoupled fast adaptation and robustness. The \mathcal{L}_1 -MPC consists of two parts: the nominal MPC and the \mathcal{L}_1 adaptive controller, where the \mathcal{L}_1 adaptive controller makes the real system act as the nominal reference model, and the nominal MPC predicts the future system behavior based on the nominal reference model and solves for the optimal control values. The \mathcal{L}_1 adaptive controller is inserted between the actual plant and the nominal MPC.

As illustrated in fig. 5, the control output of the nominal MPC acts on the combined system, where the \mathcal{L}_1 adaptive controller takes care of the model mismatch and external disturbances and converges the dynamics of the combined system to the nominal dynamics. As a result, we no longer need to fine-tune the parameters of the MPC reference model.

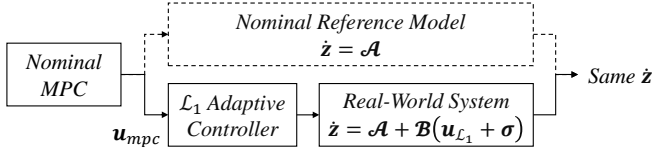


Fig. 5. An overview of the \mathcal{L}_1 -MPC methodology. See (10) for symbol definitions.

A model predictive controller is an optimization-based controller that solves optimal control problems (OCP) in a receding-horizon fashion. We formulate the OCP as follows:

$$\begin{aligned} \min_{[u_0 \dots u_{N-1}]} & \sum_{k=0}^{N-1} (e_k^\top Q e_k + u_k^\top R u_k) + e_N^\top Q_N e_N \\ \text{s.t.} & \begin{cases} h_k \in [h_{lb}, h_{ub}] \\ u_k \in [u_{lb}, u_{ub}] \\ \dot{x} = \text{dyn}(x, u) \\ x_0 = x(t) \end{cases} \end{aligned} \quad (6)$$

where

$$x = \begin{bmatrix} p \\ q \\ w^v \\ B\omega \\ Bf_a \\ B\tau_a \end{bmatrix}, \quad u = \begin{bmatrix} B\dot{f}_a \\ B\dot{\tau}_a \end{bmatrix}, \quad e = \begin{bmatrix} p_{err} \\ q_{err} \\ w^v_{err} \\ B\omega_{err} \\ Bf_a \\ B\tau_a \end{bmatrix}, \quad h = \begin{bmatrix} w^v \\ F \end{bmatrix} \quad (7)$$

$$q \otimes q_{ref}^{-1} = \begin{bmatrix} w \\ q_{err} \end{bmatrix}$$

The state vector includes the wrench to be produced by actuators. With the time derivative of the actuator wrench as the control vector, we can explicitly apply constraints on the wrench changing rate and implicitly limit the tilt angle rotation speeds [7]. The position error p_{err} , velocity error w^v_{err} , and angular velocity error $B\omega_{err}$ are the difference between the reference value and current value. The quaternion error is calculated using the quaternion product. Vector h is composed of values constrained by an upper and a lower bound, and the rotor thrust F vector is obtained by the Moore–Penrose inverse of a force allocation matrix B .

$$\begin{aligned} y &\triangleq B^\dagger \begin{bmatrix} Bf_a \\ B\tau_a \end{bmatrix} = [y_1, \dots, y_{12}]^\top \\ F &= [y_1^2 + y_2^2, \dots, y_{11}^2 + y_{12}^2]^\top \end{aligned} \quad (8)$$

The nonlinear model $\dot{x} = \text{dyn}(x, u)$ is fully expanded to:

$$\dot{x} = \begin{bmatrix} w^v \\ \frac{1}{2}q \otimes \begin{bmatrix} 0 \\ B\omega \end{bmatrix} \\ g + \frac{1}{m} \text{rotate}(Bf_a, q) \\ J^{-1}(B\tau_a - B\hat{d}_{com} \times Bf_a - B\omega \times (J \cdot B\omega)) \\ B\dot{f}_a \\ B\dot{\tau}_a \end{bmatrix} \quad (9)$$

In designing the \mathcal{L}_1 adaptive controller, uncertainties only appear as additional wrench added to the system dynamics. So let $\dot{z} = [w^v, B\omega]^\top$ and consider the uncertainties, we

can describe the system behavior in terms of ideal dynamics \mathcal{A} and dynamics caused by the uncertainties \mathcal{B} :

$$\begin{aligned} \dot{z} &= \begin{bmatrix} g + \frac{1}{m} \text{rotate}(Bf_a, q) \\ J^{-1}(B\tau_a - B\hat{d}_{com} \times Bf_a - B\omega \times (J \cdot B\omega)) \\ J^{-1} \begin{bmatrix} R \\ B\hat{d}_{com} \end{bmatrix} \begin{bmatrix} Bf_{L1} \\ B\tau_{L1} \end{bmatrix} + \begin{bmatrix} Bf_\Delta \\ B\tau_\Delta \end{bmatrix} \end{bmatrix} \\ &\triangleq \mathcal{A} + \mathcal{B}(u_{L1} + \sigma) \end{aligned} \quad (10)$$

where R is the rotation matrix that corresponds to the attitude quaternion, and $B\hat{d}_{com}$ is the skew-symmetric matrix of $B\hat{d}_{com}$.

In [14] and [15], uncertainties are divided into matched and unmatched parts. Because the actuators of a quadrotor cannot generate forces on its XY plane, the corresponding force uncertainties are called unmatched uncertainties. For the OMAV case, all uncertainties are matched uncertainties. According to the \mathcal{L}_1 adaptive control theory, the state predictor is:

$$\dot{\hat{z}} = \mathcal{A} + \mathcal{B}(u_{L1} + \hat{\sigma}) + A\tilde{z} \quad (11)$$

where $\tilde{z} = \hat{z} - z$, and $\hat{*}$ means the estimated value of $*$. $\hat{\sigma}$ is estimated by the adaptive control law, which is given in discrete-time form as:

$$\hat{\sigma}_k = -\mathcal{B}^{-1}(e^{AT_s} - I_6)^{-1} A e^{AT_s} \tilde{z}_k \quad (12)$$

The matrix exponential e^{AT_s} refers to the discretized state matrix that corresponds to matrix A . Matrix A is a Hurwitz matrix, and it also represents the adaptive gain. Moreover, Matrix A is often set to a diagonal matrix with all negative elements in practice. For an element on the diagonal line, the bigger its absolute value is, the higher adaptive gain it represents. With high adaptive gains, the estimation of $\hat{\sigma}$ is faster, and the system is more responsive to external disturbances. Nevertheless, high gains tend to bring high-frequency oscillation to $\hat{\sigma}$, so to get smooth compensation, a low pass filter is introduced:

$$u_{L1} = -\text{LPF}(\hat{\sigma}) \quad (13)$$

Till now, we can present the complete \mathcal{L}_1 -MPC algorithm:

Algorithm 1: The \mathcal{L}_1 -MPC algorithm

```

 $\hat{z}_0 \leftarrow z_0$ ;
 $u_{mpc,-1} \leftarrow 0$ ;
 $T_s \leftarrow$  control period;
while  $k \geq 0$  do
     $u_{ocp} \leftarrow$  optimal wrench rates from OCP solver;
     $u_{mpc,k} \leftarrow u_{mpc,k-1} + u_{ocp}T_s$ ;
    update  $\mathcal{A}$ ,  $\mathcal{B}$ ,  $z$ , and  $\tilde{z}_k$ ;
     $\hat{\sigma}_k \leftarrow -\mathcal{B}^{-1}(e^{AT_s} - I_6)^{-1} A e^{AT_s} \tilde{z}_k$ ; // (12)
     $u_{L1,k} \leftarrow -\text{LPF}(\hat{\sigma}_k)$ ; // (13)
    output  $u_{L1,k} + u_{mpc,k}$  to the control allocator;
     $\hat{z}_k \leftarrow \mathcal{A} + \mathcal{B}(u_{L1,k} + \hat{\sigma}_k) + A\tilde{z}_k$ ; // (11)
     $\hat{z}_{k+1} \leftarrow \hat{z}_k + T_s \hat{z}_k$ ;
     $k \leftarrow k + 1$ 
end

```

Note that \mathcal{B}^{-1} is calculated in each loop at step four. To reduce the computational overhead, using the property of rotation matrices $\mathbf{R} \in \text{SO}(3)$, the inverse operation is transformed into:

$$\begin{bmatrix} \frac{\mathbf{R}}{m} & \mathbf{0} \\ \mathbf{J}^{-1} \frac{d}{dt} \hat{\mathbf{d}}_{com} & \mathbf{J}^{-1} \end{bmatrix}^{-1} = \begin{bmatrix} m\mathbf{R}^\top & \mathbf{0} \\ m \frac{d}{dt} \hat{\mathbf{d}}_{com} \mathbf{R}^\top & \mathbf{J} \end{bmatrix} \quad (14)$$

Additionally, the inverse of inertia \mathbf{J}^{-1} and the constant value in (12): $(e^{A\tau_s} - \mathbf{I}_6)^{-1}$ can be pre-calculated at controller initialization.

B. PID Backup Control

Optimization-based controllers suffer from robustness and convergence issues when the current states are too far from the desired trajectory. No updated wrench command is available if the OCP cannot be solved. We use a classical PID-based backup controller to address this issue. The controller can also function as a standalone controller. The algorithm is modified upon the one given in the PX4 project.

The position controller and attitude controller run in parallel to calculate the acceleration setpoint ${}_W\dot{\mathbf{v}}_{sp}$ and the angular acceleration setpoint ${}_B\dot{\boldsymbol{\omega}}_{sp}$. The position controller consists of an outer position loop and an inner velocity loop. The attitude controller comprises a nonlinear quaternion-based controller [17] and an inner angular velocity loop. When the PID controller is activated, the body wrench command is calculated using the acceleration setpoints in (15). Otherwise, the wrench command comes from the adaptive MPC.

$$\begin{aligned} {}_B\mathbf{f}_a &= m(\text{rotate}({}_W\dot{\mathbf{v}}_{sp} - \mathbf{g}, \mathbf{q}^{-1}) + {}_B\boldsymbol{\omega} \times \text{rotate}({}_W\mathbf{v}, \mathbf{q}^{-1})) \\ {}_B\boldsymbol{\tau}_a &= \mathbf{J} \cdot {}_B\dot{\boldsymbol{\omega}}_{sp} + {}_B\mathbf{d}_{com} \times {}_B\mathbf{f}_a + {}_B\boldsymbol{\omega} \times (\mathbf{J} \cdot {}_B\boldsymbol{\omega}) \end{aligned} \quad (15)$$

C. Control Allocation

For this part, the results [2]–[4] are directly used. The control allocation algorithm returns a least-square solution using the pseudo-inverse matrix calculation. Measures for handling kinematics singularities are implemented.

In the first step, we move the variables in the allocation matrix \mathbf{M} to a temporary vector \mathbf{U} :

$$\begin{bmatrix} {}_B\mathbf{f}_a \\ {}_B\boldsymbol{\tau}_a \end{bmatrix} = \mathbf{M}_c \mathbf{U} = \mathbf{M}_c [\Omega_1^2 s_1, \Omega_1^2 c_1, \dots, \Omega_6^2 s_6, \Omega_6^2 c_6]^\top \quad (16)$$

where s_i denotes $\sin \alpha_i$ and c_i denotes $\cos \alpha_i$. To compute the least-square solution, we use the Moore–Penrose inverse in the second step:

$$\mathbf{U} = \mathbf{M}_c^\dagger \begin{bmatrix} {}_B\mathbf{f}_a \\ {}_B\boldsymbol{\tau}_a \end{bmatrix} \quad (17)$$

Finally, to extract individual actuator commands from \mathbf{U} , we follow these equations:

$$\Omega_i = \sqrt{(\Omega_i^2 s_i)^2 + (\Omega_i^2 c_i)^2}, \quad \alpha_i = \tan^{-1} \left(\frac{\Omega_i^2 s_i}{\Omega_i^2 c_i} \right) \quad (18)$$

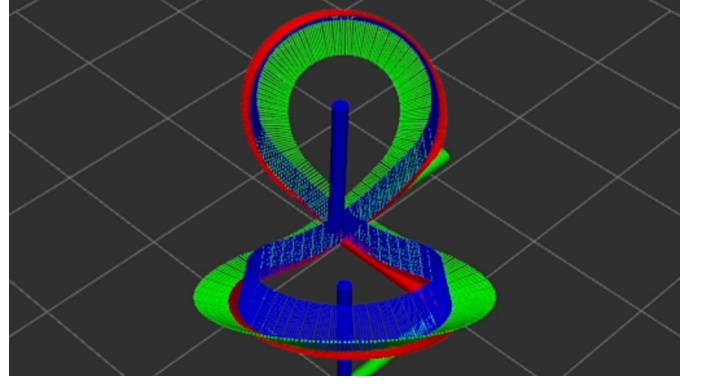


Fig. 6. Illustration of the reference trajectory. Its XYZ and Euler Angle representation is presented in fig. 9

IV. EXPERIMENTS

A. Settings

We build prototypes of the OCP solver and EKF in Python using CasADi [18] and acados [19]. Then we implement the controllers as optimized C++ ROS2 nodes with the generated code. The OCP formulation's time horizon is 1 second with $N = 20$. The \mathcal{L}_1 -MPC and EKF-MPC run at 100 Hz. We select a 6-DOF trajectory (fig. 6) that is almost impossible for underactuated MAVs to track.

The OCP formulation for EKF-MPC is almost the same as the one used in the \mathcal{L}_1 -MPC. The only difference is that the dynamics equations in (9) are modified into:

$$\begin{bmatrix} \mathbf{g} + \frac{1}{m} \text{rotate}({}_B\mathbf{f}, \mathbf{q}) \\ \mathbf{J}^{-1}({}_B\boldsymbol{\tau} - {}_B\mathbf{d}_{com} \times {}_B\mathbf{f} - {}_B\boldsymbol{\omega} \times (\mathbf{J} \cdot {}_B\boldsymbol{\omega})) \end{bmatrix} \quad (19)$$

where ${}_B\mathbf{f} = {}_B\mathbf{f}_a + {}_B\mathbf{f}_{EKF}$, ${}_B\boldsymbol{\tau} = {}_B\boldsymbol{\tau}_a + {}_B\boldsymbol{\tau}_{EKF}$, and the force and torque with the EKF subscript are estimated by the EKF.

The states \mathbf{x}_{EKF} , system input \mathbf{u}_{EKF} and observation vector \mathbf{z}_{EKF} of the EKF are defined as:

$$\mathbf{x}_{EKF} = \begin{bmatrix} \mathbf{p} \\ \mathbf{q} \\ {}_W\mathbf{v} \\ {}_B\boldsymbol{\omega} \\ {}_B\mathbf{f}_{EKF} \\ {}_B\boldsymbol{\tau}_{EKF} \end{bmatrix}, \quad \mathbf{u}_{EKF} = \begin{bmatrix} {}_B\mathbf{f}_a \\ {}_B\boldsymbol{\tau}_a \end{bmatrix}, \quad \mathbf{z}_{EKF} = \begin{bmatrix} \mathbf{p} \\ \mathbf{q} \\ {}_W\mathbf{v} \\ {}_B\boldsymbol{\omega} \end{bmatrix} + \mathbf{v}_{EKF} \quad (20)$$

And the system dynamics is:

$$\dot{\mathbf{x}}_{EKF} = \begin{bmatrix} {}_W\mathbf{v} \\ \frac{1}{2} \mathbf{q} \otimes \begin{bmatrix} 0 \\ {}_B\boldsymbol{\omega} \end{bmatrix} \\ \mathbf{g} + \frac{1}{m} \text{rotate}({}_B\mathbf{f}, \mathbf{q}) \\ \mathbf{J}^{-1}({}_B\boldsymbol{\tau} - {}_B\mathbf{d}_{com} \times {}_B\mathbf{f} - {}_B\boldsymbol{\omega} \times (\mathbf{J} \cdot {}_B\boldsymbol{\omega})) \\ - {}_B\dot{\boldsymbol{\omega}} \cdot {}_B\mathbf{f}_{EKF} \\ \mathbf{0} \end{bmatrix} + \mathbf{w}_{EKF} \quad (21)$$

where \mathbf{v}_{EKF} is the observation noise and \mathbf{w}_{EKF} is the process noise; they are both column vectors. Since the dynamics of disturbances are not easy to model, we assume ${}_W\dot{\mathbf{f}}_{EKF} = {}_B\dot{\mathbf{f}}_{EKF} = \mathbf{0}$ as suggested in [7], it follows the product rule for differentiation, then we get ${}_B\dot{\mathbf{f}}_{EKF} = -{}_B\dot{\boldsymbol{\omega}} \cdot {}_B\mathbf{f}_{EKF}$. To

estimate fast-changing time-variant disturbances, we set the corresponding values in the process noise covariance matrix to a relatively high value.

The EKF algorithm is presented in [20] for practical implementation. Equation (21) is discretized in the algorithm using the Runge-Kutta 4th order method.

B. Numerical Simulation

Numerical simulation is done with the numerical integrators acting as the Omnihex. We manually tweak the model referenced in the integrator so that we can evaluate how the \mathcal{L}_1 -MPC improves tracking accuracy. We evaluate tracking accuracy by the position root mean square error (RMSE) and quaternion RMSE.

We divide the experiments into four groups: A, B, C, and D. Each group uses the same integrator model but different controllers. The specific integrator models used are:

- A: nominal model,
- B: mass reduced by 0.5 Kg, inertia reduced by 50%, the center of mass moved $\sqrt{3}$ cm away from the original,
- C: mass increased by 0.5 Kg, inertia doubled, the center of mass moved $\sqrt{3}$ cm away from the original,
- D: mass increased by 0.5 Kg, inertia doubled, the center of mass moved $\sqrt{3}$ cm away from the original, and extra disturbance is applied (22, 23).

And subscripts denote the type of controllers:

- 1: the nominal MPC,
- 2: the \mathcal{L}_1 -MPC,
- 3: the EKF-MPC.

The dynamics equations for the integrator in group D are:

$$\begin{bmatrix} {}_W\dot{\mathbf{p}} \\ {}_B\dot{\boldsymbol{\omega}} \end{bmatrix} = \begin{bmatrix} \mathbf{g} + \frac{1}{m}\text{rotate}({}_B\mathbf{f}_a + \sin({}_B\mathbf{f}_a)), \mathbf{q} \\ \mathbf{J}^{-1}\mathbf{T} \end{bmatrix} \quad (22)$$

where

$$\begin{aligned} \mathbf{T} &= 0.9({}_B\boldsymbol{\tau}_a + \sin({}_B\boldsymbol{\tau}_a)) \\ &\quad - 0.95{}_B\mathbf{d}_{com} \times {}_B\mathbf{f}_a \\ &\quad - {}_B\boldsymbol{\omega} \times (\mathbf{J} \cdot {}_B\boldsymbol{\omega}) \end{aligned} \quad (23)$$

Simulation results are shown in fig. 7 to fig. 10.

Fig. 7 shows the performance comparison of the \mathcal{L}_1 -MPC and the nominal MPC on different integrator models when tracking trajectories of different periods. As the period decreases, the average velocity increases, and the tracking errors increase. Nevertheless, the \mathcal{L}_1 -MPC reduces both the position tracking RMSE and quaternion tracking RMSE by around 90%. Fig. 8 presents the results for the EKF-MPC in the same fashion.

As shown in fig. 8, the EKF-MPC does not perform as well as the \mathcal{L}_1 -MPC. When the trajectory period is 15 seconds, the RMSE down percentage for position tracking is decreased to roughly 50%, which can be explained by fig. 9 and fig. 10. Fig. 9 shows the time-domain data of Group D with a period equal to 15 seconds. The nominal controller completely fails in roll and pitch tracking and exhibits a constant offset in height tracking, while the \mathcal{L}_1 -MPC can track the trajectory on each DOF perfectly. The EKF-MPC performs in general as well as the \mathcal{L}_1 -MPC; however, it only achieves offset-free height

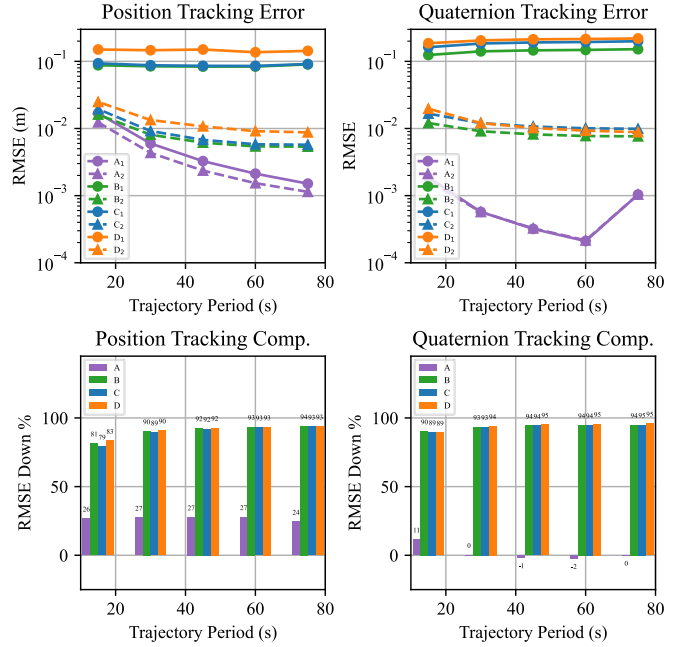


Fig. 7. Tracking RMSE reduction using the \mathcal{L}_1 -MPC.

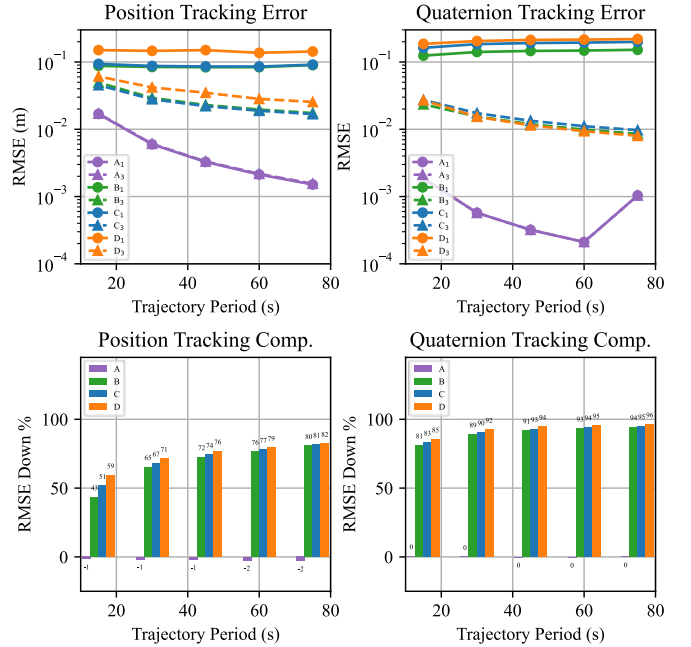


Fig. 8. Tracking RMSE reduction using the EKF-MPC.

tracking after 4 seconds since the start. The direct reason is that the estimation rate of EKF is not tuned as high as the \mathcal{L}_1 adaptive rate. With larger covariance for the process noises, the lines of EKF-MPC in fig. 10 move closer to the lines of \mathcal{L}_1 -MPC, but setting high covariance tends to introduce higher spikes and make the system more sensitive, or less robust, to noises.

C. Gazebo Simulation

In the Gazebo simulation, we compare the results of the nominal MPC, the \mathcal{L}_1 -MPC, the EKF-MPC, and the PID-

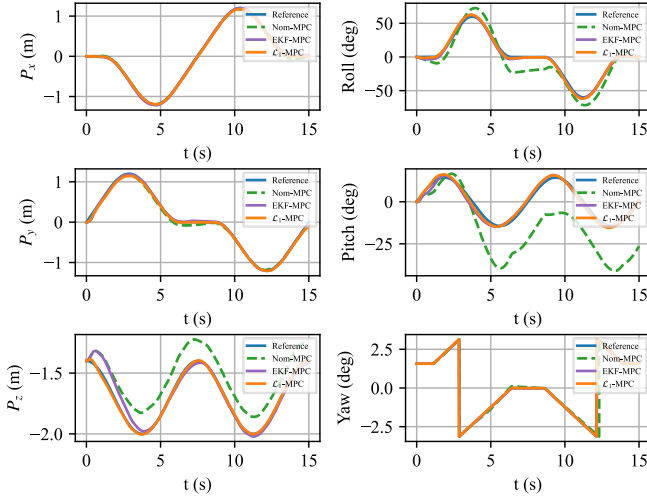


Fig. 9. Reference and actual trajectory (D, period: 15s).

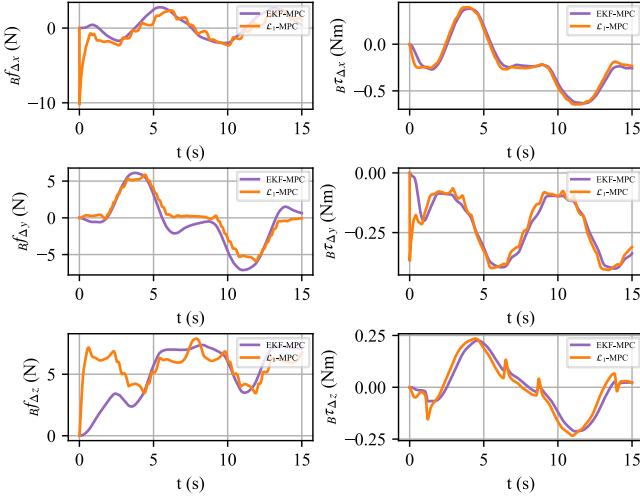


Fig. 10. Estimated wrench uncertainties (D, period: 15s).

based controller (running in PX4 offboard mode). To introduce model mismatch to the model simulated in Gazebo, we use a motor plugin that generates more unmodeled forces and torques and tweaks the allocation algorithm:

$$\Omega_i = \sqrt[4]{(\Omega_i^2 s_i)^2 + (\Omega_i^2 c_i)^2} \rightarrow \Omega_i = \sqrt[2]{(\Omega_i^2 s_i)^2 + (\Omega_i^2 c_i)^2} \quad (24)$$

We conduct tracking experiments on trajectories of the same shape but in different periods. The tracking errors, RMSE reduction, and the actual trajectory are plotted in fig. 11 and fig. 11.

Fig. 11 shows the good overall performance of the PID controller. However, since the PID controller is entirely reactive and does not look into the future in the time horizon, the tracking errors increase by a large percentage as the average speed increases. The nominal MPC operates with the nominal parameters calculated using the CAD file; It looks into the future but predicts the system's behavior based on the inaccurate model, only to make tracking errors even larger. While both the \mathcal{L}_1 -MPC and the EKF-MPC improve tracking performance, the EKF-MPC tends to have a slower estimation

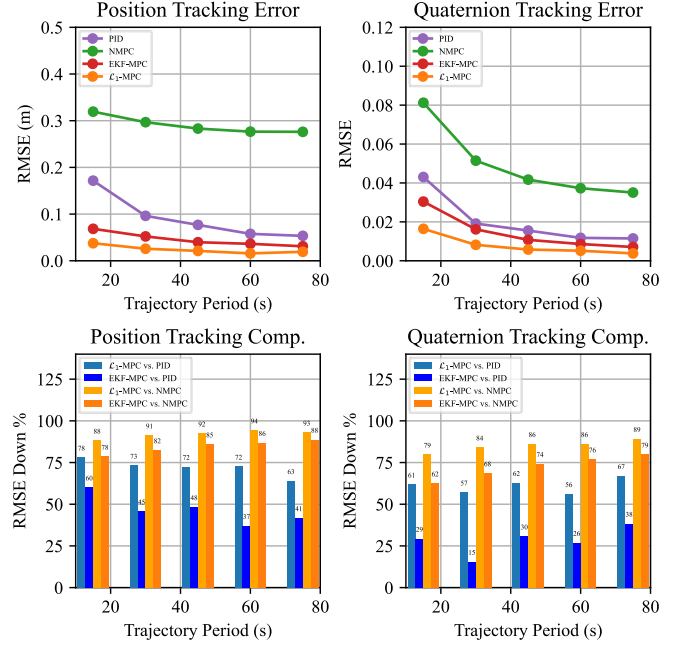


Fig. 11. Tracking RMSE reduction of the \mathcal{L}_1 -MPC and the EKF-MPC.

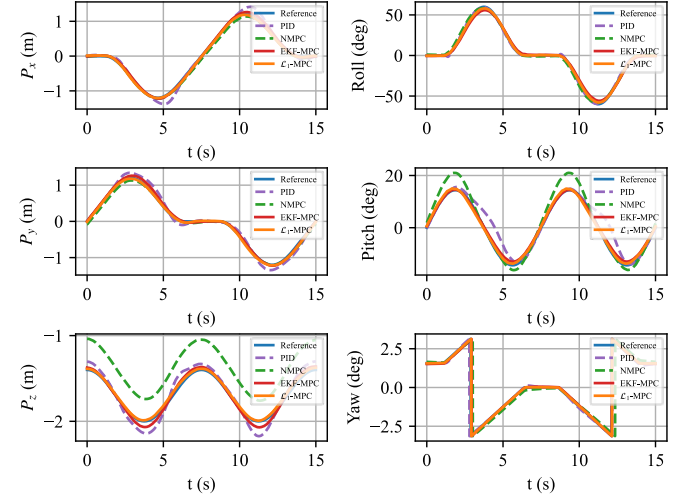


Fig. 12. Reference trajectory and actual trajectory (period: 15s).

rate, resulting in larger RMSEs. Setting large covariances of the process noise brings oscillation to the system and makes the system unstable. In fig. 12, On sharp turns, the EKF-MPC cannot track the reference precisely, as seen in experiments in [7]. In addition, the average time used for optimization is 1.3 microseconds (Core-i7 11800H, Ubuntu 20.04 WSL), and the time needed to update the \mathcal{L}_1 controller or the EKF is negligible.

We also notice that in the Gazebo simulation experiments, the handling of kinematics singularities impedes tracking. Suppose the maximum value of the Roll trajectory reaches 90 degrees. In that case, the desired course of tilting angles becomes discontinuous due to the singularity-handling algorithms [4] modifying the tilt angle setpoints. The singularity-handling algorithms introduce a threshold for the angle between the

body force vector and vehicle arm vectors. When the angle is within the threshold, the tilt angle rates of the corresponding arms are ramped down to zero after the actual desired rates are calculated. As a result, the desired actuator commands are not executed, thus impeding trajectory tracking.

V. DISCUSSION

Since we use the PX4 SITL framework with Gazebo, the controller implementations can be directly deployed on an actual physical Omnihex with a few extra tunings. As the adaptive MPCs can adapt to model mismatches, including imprecise model parameters, only controller gains need to be tuned. For the \mathcal{L}_1 -MPC, we only need to tune the adaptive gain matrix and the cut-off frequencies of the low pass filter. However, for the EKF-MPC, we have two covariance matrices to tune. It is harder to get a set of parameters that enable high estimation rates while preserving system stability.

The problem of the \mathcal{L}_1 -MPC lies in its cascaded architecture, which allows the adaptive layer to break constraints, while the problem of the EKF-MPC is that it is hard to achieve fast estimation without introducing excessive oscillation. We assume that the \mathcal{L}_1 -MPC can be improved by adopting methods of the EKF-MPC and vice versa. For example, we may use the \mathcal{L}_1 adaptive controller as a pure estimator to eliminate the potential of breaking constraints and integrate the estimated uncertainties into the OCP formulation. Also, we may add an LPF to the EKF-MPC to decouple the estimation rate from robustness similarly. In addition, we hypothesize that integrating the control allocation and singularity handling into the OCP formulation will further reduce the tracking error. These are excellent topics for future research.

For the PID controller, one aspect that can be improved is that the gains for the nonlinear quaternion-based attitude controller should be changed online according to the configuration of arm tilt angles. Because at different configurations, the dynamics of rotation are different.

VI. CONCLUSION

Aimed at achieving accurate trajectory tracking on the Omnihex platform, whose precise model is challenging to obtain, we present the \mathcal{L}_1 -MPC, together with a backup controller plan, and the implementation of the EKF-MPC. The \mathcal{L}_1 -MPC and EKF-MPC are both adaptive methods that can significantly reduce the adverse effects of imprecise model parameters, unmodeled dynamics, and external disturbances. Nevertheless, the simulated experiments show that the \mathcal{L}_1 -MPC is better regarding lower tracking errors, higher uncertainty estimation rates, and fewer tuning efforts.

We look forward to deploying the proposed \mathcal{L}_1 -MPC on a real-world Omnihex. Hopefully, they are potentially helpful in tasks requiring accurate trajectory tracking abilities, such as flying through a narrow gap, or in tasks requiring disturbance rejection, such as flying with a robotic arm for aerial manipulation.

REFERENCES

- [1] M. Hamandi, F. Usai, Q. Sablé, N. Staub, M. Tognon, and A. Franchi, "Design of multirotor aerial vehicles: A taxonomy based on input allocation," *The International Journal of Robotics Research*, vol. 40, no. 8-9, pp. 1015–1044, 2021.
- [2] O. Elkhatab, "Control allocation of a tilting rotor hexacopter," Bachelor Thesis, ETH Zurich, Zurich, 2017.
- [3] M. Kamel, S. Verling, O. Elkhatab, C. Sprecher, P. Wulkop, Z. Taylor, R. Siegwart, and I. Gilitschenski, "The voliro omniorientational hexacopter: An agile and maneuverable tiltable-rotor aerial vehicle," *IEEE Robotics & Automation Magazine*, vol. 25, no. 4, pp. 34–44, 2018.
- [4] K. Bodie, Z. Taylor, M. Kamel, and R. Siegwart, "Towards efficient full pose omnidirectionality with overactuated mavs," in *Proceedings of the 2018 International Symposium on Experimental Robotics*, J. Xiao, T. Kröger, and O. Khatib, Eds. Cham: Springer International Publishing, 2020, pp. 85–95.
- [5] M. Allenspach, K. Bodie, M. Brunner, L. Rinsoz, Z. Taylor, M. Kamel, R. Siegwart, and J. Nieto, "Design and optimal control of a tiltrotor micro-aerial vehicle for efficient omnidirectional flight," *The International Journal of Robotics Research*, vol. 39, no. 10-11, pp. 1305–1325, 2020.
- [6] W. Zhang, M. Brunner, L. Ott, M. Kamel, R. Siegwart, and J. Nieto, "Learning dynamics for improving control of overactuated flying systems," *IEEE Robotics and Automation Letters*, vol. 5, no. 4, pp. 5283–5290, 2020.
- [7] M. Brunner, K. Bodie, M. Kamel, M. Pantic, W. Zhang, J. Nieto, and R. Siegwart, "Trajectory tracking nonlinear model predictive control for an overactuated mav," in *2020 IEEE International Conference on Robotics and Automation (ICRA)*, 2020, pp. 5342–5348.
- [8] L. Peric, M. Brunner, K. Bodie, M. Tognon, and R. Siegwart, "Direct force and pose nmpe with multiple interaction modes for aerial push-and-slide operations," in *2021 IEEE International Conference on Robotics and Automation (ICRA)*, 2021, pp. 131–137.
- [9] N. Hovakimyan and C. Cao, *\mathcal{L}_1 Adaptive Control Theory: Guaranteed Robustness with Fast Adaptation*. USA: Society for Industrial and Applied Mathematics, 2010.
- [10] E. Xargay, N. Hovakimyan, and C. Cao, " \mathcal{L}_1 adaptive controller for multi-input multi-output systems in the presence of nonlinear unmatched uncertainties," in *Proceedings of the 2010 American Control Conference*, 2010, pp. 874–879.
- [11] E. Kharisov, N. Hovakimyan, J. Wang, and C. Cao, " \mathcal{L}_1 adaptive controller for time-varying reference systems in the presence of unmodeled nonlinear dynamics," in *Proceedings of the 2010 American Control Conference*, 2010, pp. 886–891.
- [12] Z. Li and N. Hovakimyan, " \mathcal{L}_1 adaptive controller for mimo systems with unmatched uncertainties using modified piecewise constant adaptation law," in *2012 IEEE 51st IEEE Conference on Decision and Control (CDC)*, 2012, pp. 7303–7308.
- [13] K. Pereida and A. P. Schoellig, "Adaptive model predictive control for high-accuracy trajectory tracking in changing conditions," in *2018 IEEE/RSJ International Conference on Intelligent Robots and Systems (IROS)*, 2018, pp. 7831–7837.
- [14] J. Pravitra, K. A. Ackerman, C. Cao, N. Hovakimyan, and E. A. Theodorou, " \mathcal{L}_1 -adaptive mppi architecture for robust and agile control of multirotors," in *2020 IEEE/RSJ International Conference on Intelligent Robots and Systems (IROS)*, 2020, pp. 7661–7666.
- [15] D. Hanover, P. Foehn, S. Sun, E. Kaufmann, and D. Scaramuzza, "Performance, precision, and payloads: Adaptive nonlinear mpc for quadrotors," *IEEE Robotics and Automation Letters*, vol. 7, pp. 690–697, 2022.
- [16] J. Diebel, "Representing attitude: Euler angles, unit quaternions, and rotation vectors," *Matrix*, vol. 58, 01 2006.
- [17] D. Brescianini, M. Hehn, and R. D'Andrea, "Nonlinear quadcopter attitude control. technical report," Eidgenössische Technische Hochschule Zürich, Zürich, Report, 2013.
- [18] J. Andersson, J. Gillis, G. Horn, J. B. Rawlings, and M. Diehl, "Casadi: a software framework for nonlinear optimization and optimal control," *Mathematical Programming Computation*, vol. 11, pp. 1–36, 2019.
- [19] R. Verschuere, G. Frison, D. Kouzoupis, J. Frey, N. van Duijkeren, A. Zanelli, B. Novoselnik, T. Albin, R. Quirynen, and M. Diehl, "acados—a modular open-source framework for fast embedded optimal control," *Mathematical Programming Computation*, vol. 14, pp. 147–183, 2022.
- [20] Q. Quan, *Introduction to multicopter design and control*. Springer, 2017.